nature climate change

SUPPLEMENTARY INFORMATION

DOI: 10.1038/NCLIMATE2635

Unabated global mean sea-level rise over the satellite altimeter era

Watson, C.S., White, N.J., Church, J.A., King, M.A., Burgette, R.J. and Legresy, B.

Contents

Supplementary Methods....2
- Tide Gauge and Altimeter Sea Surface Height Data....2
- Vertical Land Movement Data....2
- Validation Approach....4
- Mission-wise Analysis and Error Estimates....7
- GMSL Analysis and Error Estimates....8

Supplementary Discussion....9
- Characterisation and Attribution of the TOPEX Side A Bias Drift....9
- TOPEX Side A/B Intra-mission Relative Bias....13
- Inter-mission Relative Biases....13
- Bias Drift Sensitivity....14
- Multi-mission Ensemble Bias Drift Determination....16
- GMSL Comparisons....17

Supplementary References....19

Supplementary Methods

Tide Gauge and Altimeter Sea Surface Height Data

We use hourly tide gauge data from the 'fast-GLOSS' (Global Sea Level Observing System) network, distributed via the University of Hawaii Sea Level Centre (UHSLC, http://uhslc.soest.hawaii.edu/). These data are supplemented with hourly data from additional sites from the Australian National Tidal Centre (NTC, http://www.bom.gov.au/oceanography/projects/abslmp/data/). Preference is given to the records commencing at, or prior, to the launch of T/P (August 1992). 77% of TGs meet this threshold, while 97% of TGs commenced prior to the switch between T/P side-A and B (February, 1999). 83% of TGs run for 20 years or longer.

Altimeter SSH is derived using 1-Hz along-track GDR altimeter data from solely the "Jason-class" reference missions; TOPEX/Poseidon (T/P), Jason-1 and OSTM/Jason-2. For the T/P mission, we limit our analysis to TOPEX data given limited utilisation of the Poseidon altimeter. We commence our processing using all available MGDR-B[30] and GDR-C[27] data for T/P and Jason-1 respectively, and GDR-D[28] data for OSTM/Jason-2, for the period 1993 to mid-2014. We process using the standard edits and checks comparable to those described by ref 32 (including important corrections for the TOPEX microwave radiometer (TMR) following ref 29, and enhancements for the Jason microwave radiometer (JMR) following ref 31) and as recommended in the relevant product documentation[27,28,30]. For the sea state bias (SSB) model, we adopt the Chambers et al. sea state bias (SSB) model for TOPEX[33], and the Tran et al. model[34] for Jason-1 and OSTM/Jason-2. GSFC1204 and GSFC1404 orbits (for TOPEX/Jason-1 and OSTM/Jason-2 respectively, updated from ref 35) are used, each with the same reference frame (ITRF2008[21]) across all missions. We remove deformation of the solid Earth from the altimeter SSH (the solid Earth tide, ocean tide loading and pole tide), but do not remove the ocean tide nor apply an inverse barometer correction at this stage of the analysis.

Vertical Land Movement Data

Our VLM trends are an update of those of ref 18, using an identical analysis strategy but making use of GPS sites within public archives and up to 100 km from each of the TGs. Data spanning from 1995 to mid-2013 were homogeneously analysed to derive daily time series. We estimated the linear trend simultaneously with annual and semi-annual periodic terms, offsets and appropriate treatment of time series autocorrelation using noise parameters that describe a time-

variable white plus power law noise model[36]. We assume the linear motion is representative of the VLM over the duration of the altimeter period, despite different data durations at each site. Sites that exhibit clear non-linear VLM (e.g. due to ground water extraction or elastic rebound associated with nearby ice mass loss) are flagged for later exclusion. We include sites with at least 1.5 years of data, but only include estimates of VLM that are well resolved with uncertainties less than 1 mm/yr (effectively limiting the number of sites with VLM estimated from short records). Comparison of our GPS derived VLM to an independent GPS dataset[25] at 71 overlapping sites yields a mean difference of -0.13 mm/yr with WRMS of 0.7 mm/yr (computed as our solution minus the solution of ref 25). We note that a lower mean VLM has the effect of a positive shift in the estimated bias drift and thus a decrease in the adjusted rate of change in GMSL.

Given a TG may have multiple GPS sites located within 100 km, we compute a weighted mean of the GPS VLM. The weights are chosen with the aim of achieving a reasonable balance between GPS VLM uncertainty and the distance from each GPS to the TG. Here, the weight given to each GPS site is a product of two weights ($W=W_1W_2$). First, we define a weight (W_1) based on the separation distance (d; in km) between the GPS and TG, such that at 0 km separation the weight is 1, reducing according to Eqn 2 to 0.5 at 100 km.

$$W_1 = 0.5\cos(2\pi\, d/400) + 0.5 \qquad \text{Eqn 2}$$

Second, we define W_2 based on the VLM uncertainty (σ, mm/yr) that is constant with small σ and then tapers linearly to zero:

$$W_2 = \begin{cases} 1 & if\ \sigma \leq 0.2 \\ -1.25\sigma + 1.25 & if\ 0.2 < \sigma < 1 \\ 0 & if\ \sigma \geq 1 \end{cases} \qquad \text{Eqn 3}$$

Note that this strategy does not allow for reduction in the weight of a GPS as a function of distance in the case of having a single GPS within 100 km (i.e. the distance dependent term (Eqn 2) only takes effect when multiple GPS are present within 100 km). We note that approximately 24% of our initial TG network has GPS based VLM derived from a single site. Importantly however, 66% of these are within 5 km of the TG, 78% within 10 km and 90% within 25 km.

Where GPS velocities were not available (Supplementary Figure 1) we interpolated predicted VLM due to GIA to TG locations from the ICE-5Gv1.3_2012 (VM2) model[19]. GIA models only consider the solid earth response to past changes in glacial loading and hence do not capture other processes contributing to VLM at TGs. Large-scale regional differences are therefore evident when GIA rates are compared to GPS (e.g. ref 18), however without an independent alternative,

GIA remains the most appropriate choice in the absence of GPS. We adopt a nominal uncertainty of ± 1 mm/yr for GIA VLM estimates, slightly larger than the mean GPS uncertainty. Also tested as an alternate source of VLM is the sum of the ICE-5Gv1.3_2012 (VM2) GIA VLM estimates, and those trends derived from the Earth's elastic response to present-day mass trends determined over the period 2003-2013 using data from the GRACE mission (updated from ref 20 and linearly extrapolated over the altimeter period).

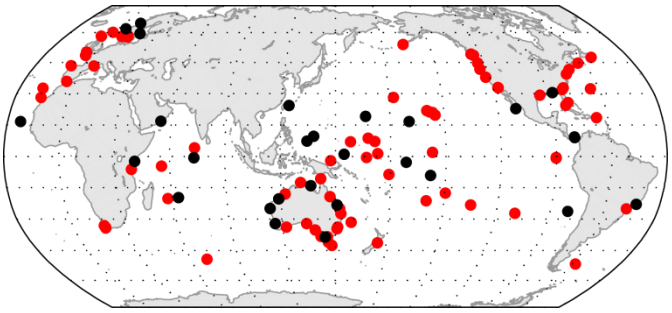

Supplementary Figure 1. TGs with (red) and without (black) GPS estimates of VLM within 100 km.

Our GPS estimates of VLM are determined with respect to the International Terrestrial Reference Frame 2008 (ITRF2008[21]), the same reference frame used for the orbits adopted for each altimeter mission (GSFC1204[35]). Unlike GPS rates, simulation studies[37] have suggested altimeter-derived GMSL trends are not sensitive to drifts in the reference frame scale-rate. However, these simulations pertain to satellite orbits defined purely by dynamical considerations, not reduced dynamic as used in all widely used altimeter orbits. Both GPS and altimeter rates used here are therefore susceptible to any such error and thus we consider these two primary datasets to be in the same frame and thus directly comparable.

Finally, we use temporally constant VLM estimates (GPS or GIA) for all missions, regardless of the time period used in the GPS analysis. We note that in the absence of further observed data, this extrapolation of GPS VLM and the elastic term added to GIA VLM will remain a limitation of the technique.

Validation Approach

For each TG, we identify all altimeter passes within 200 km of the TG (note there is a maximum of four passes per TG, with the altimeter revisiting each pass every ~9.9 days). For each candidate pass, we identify a series of offshore CPs, each separated by 20 km along the nominal ground track, out to a threshold distance of 230 km from the TG. We do this because local-scale oceanographic processes may dictate that the nearest CP may not be the most suitable

for a given TG. We eliminate any CPs where the number of valid altimeter data is < 80 % of the total number of cycles (repeat overflights) expected. Altimeter SSH is linearly interpolated to the CP, noting the across-track distance to the nominal ground track. For each CP, we form the altimeter minus TG difference (Eqn 4), correcting the relative sea level at the TG (RSL_{TG}) for VLM (linear with time *t*) . In the following expressions, superscript *Alt* denotes an altimeter mission specific term, subscript *CP* denotes a term specific to the CP, and subscript *TG* denotes a term specific to the TG. We treat TOPEX side A and side B as separate independent missions.

$$\Delta SL_{CP}^{Alt} = SSH_{CP}^{Alt} - RSL_{TG} + [VLM]_{TG}.\left(t - t_0^{Alt}\right) \qquad \text{Eqn 4}$$

The difference in sea level (ΔSL_{CP}^{Alt}) contains contributions from a number of signals including the altimeter bias drift (Eqn 5).

$$\Delta SL_{CP}^{Alt} = [Offset]_{CP}^{Alt} + [Drift]_{CP}^{Alt}.(t - t_0^{Alt}) + \cdots$$
$$\sum_{i=1}^{N}[A_i \cos(2\pi f_i t + \Phi_i)]_{CP} + [SSHSlope]_{CP}.\mathrm{d} + \varepsilon_{CP}^{Alt} \qquad \text{Eqn 5}$$

where *Offset* is a constant intercept term at time $t = t_0^{Alt}$, chosen as the mid-point time of each mission respectively; *Drift* is the altimeter bias drift term (linear with time, *t*); A_i, f_i, Φ_i are amplitude, frequency and phase of the i^{th} harmonic tidal constituents (12 in total); *SSHSlope* accounts for the SSH slope induced by the ~1 km variation in the satellite ground track location (linear with across-track distance(*d*)); and ε represents residual error that includes contributions from altimeter and TG noise and unmodelled sea-level variability between the CP and TG. We estimate the terms shown in Eqn 5 in a three-step process in order to allow independent (mission specific) treatment of time correlated noise. First, we estimate the offset, tide and across track slope terms using all available data at each CP (i.e. using all available TOPEX side A, TOPEX side B, Jason-1 and OSTM/Jason-2 in a single estimation approach). For the tidal terms, we estimate the standard 12 ocean tide constituents; SSA, MM, MF, Q1, P1, O1, K1, K2, N2, S2, M2 and M4, plus extract significant peaks in pass-based stacks of residual spectra in order to capture other dominant tidal alias periods of 1 year or less in the altimeter minus TG time series. Second, we remove the tide and across-track slope components from the time series, then solve for mission-specific offset and bias drift terms. In order to mitigate the influence of outliers, we use a robust regression approach, implemented using iteratively reweighted least squares with a bi-square weight function[38]. We estimate the drift uncertainty, $\sigma Drift_{CP}^{Alt}$, using the formal standard error statistic having scaled the parameter variance-covariance matrix by the root-mean-square-error (RMSE) squared. In order to account for time correlation in the ΔSL_{CP}^{Alt} time series, we compute the RMSE using an adjusted 'effective' number of degrees of freedom, determined

following analysis of the mission specific time series autocorrelation. Third, we correct for GPS or GIA derived VLM and add the VLM uncertainty in quadrature to the drift uncertainty.

Prior to estimating an ensemble average bias drift for each mission, we undertake quality control and thresholding. We impose a requirement that for each mission a CP must have a minimum of 70% data completeness (allowing for only a small amount of altimeter and/or tide gauge outage) to be included in subsequent analysis. To exclude highly uncertain bias drift estimates from CPs, we impose a maximum allowable value of $\sigma Drift_{CP}^{Alt}$; arbitrarily selected based on mission length to be ±10, ±15, ±9 and ±10 mm/yr for TOPEX side A, TOPEX side B, Jason-1 and OSTM/Jason-2 respectively. We also limit CPs to a maximum residual RMS (following the estimation process associated with Eqn 5) of 110 mm. We also eliminate TGs that exhibit clearly non-linear VLM, as well as TGs within an earthquake threshold. The earthquake threshold is developed using source data from the global centroid moment tensor (CMT) catalogue[39], and modeling of co-seismic displacements[40]. We derive a simple relationship using model results of global coseismic earthquake deformation for the 15 earthquakes with moment magnitude of 8.0 or greater that occurred 2000-2011[41], augmented with modelled generic earthquakes over a range of lower magnitudes. We apply this relationship to all earthquakes in the full data period, and eliminate TGs that potentially experienced a minimum of 2 mm of co-seismic vertical displacement as a result of an earthquake. This low threshold for coseismic deformation also flags sites that have experienced significant levels of post-seismic deformation. Combined, these thresholds reduce the dataset to a minimum of 90 TGs and 2200 CPs for TOPEX side A and maximum 101 TGs and 2350 CPs for Jason-1 (Supplementary Figure 2).

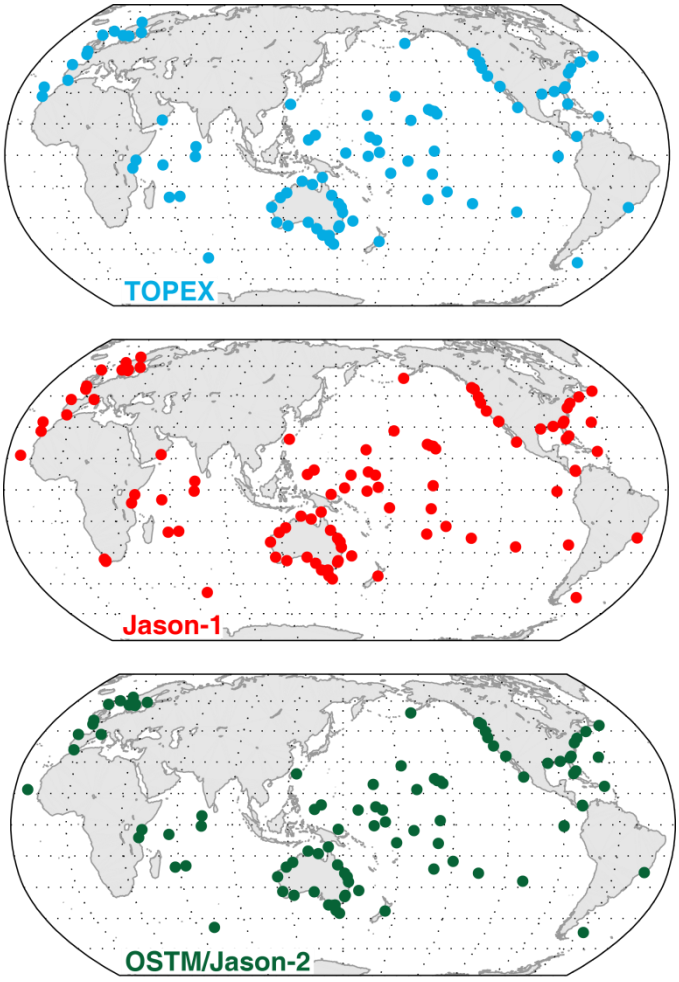

Supplementary Figure 2. TGs used in final ensemble solution for TOPEX side A and B (top), Jason-1 (middle) and OSTM/Jason-2 (bottom).

Mission-wise Analysis and Error Estimates

For each mission, we combine the CP specific bias drift terms (Eqn 5) into a weighted mean, with weights derived from $\sigma Drift_{CP}^{Alt}$ according to Eqns 6 and 7.

$$Weight_{CP}^{Alt} = 1/\left(\sigma_{CP}^{Alt}\right)^2 \qquad \text{Eqn 6}$$

$$\sigma_{CP}^{Alt} = \sqrt{\left(\sigma Drift_{CP}^{Alt}\right)^2 + \left(Q_1 : \sigma Drift_{CP}^{Alt}\right)^2} \qquad \text{Eqn 7}$$

Where Q_1 is the first quartile value of all $\sigma Drift_{CP}^{Alt}$ estimates, added in quadrature to each estimate of $\sigma Drift_{CP}^{Alt}$ in order to avoid sensitivity to very small values of $\sigma Drift_{CP}^{Alt}$. The final uncertainty of each mission specific weighted mean bias drift estimate is determined by dividing the WRMS computed from $Drift_{CP}^{Alt}$ and associated $Weight_{CP}^{Alt}$ estimates by the square root of the degrees of freedom. Noting our bias drift estimates use multiple CPs per TG and hence the

data are not independent, we estimate conservative bias drift uncertainties by adopting just one degree of freedom per TG.

Finally, we use offset and drift terms from Eqn 5 to estimate inter- and intra-mission relative biases (TOPEX side B minus TOPEX side A, Jason-1 minus TOPEX side B and OSTM/Jason-2 minus Jason-1) for each CP. We then use the same weighted average approach (Eqn 6 and 7) to generate an ensemble weighted average for each relative bias, enabling comparison with similar estimates derived from global analyses.

GMSL Analysis and Error Estimates

We derive cycle-by-cycle estimates of GMSL for each mission following the method adopted by ref 8. We correct for the predicted expansion in the ocean basin volume caused by GIA by adding +0.33 mm/yr[19], as well as correct for the well-known inverse barometric response of the ocean surface to atmospheric pressure (this correction is applied to the 1-Hz data using data from the GDR products and accepted conventions[3,30]). We apply intra- and inter-mission relative biases using the values derived as previously discussed.

In order to derive a GMSL curve adjusted for the effects of bias drift we apply the bias drift and relative bias estimates to each mission in a piecewise linear fashion. We derive the linear rate of change in GMSL by estimating it simultaneously with annual and semiannual terms using unweighted least squares. The quadratic terms are estimated using the same process, in a separate run (note the quadratic and linear terms show negligible correlation (ρ = 0.06), and the linear term varies by < 0.01 mm/yr when the quadratic term is included). Our acceleration estimates are twice the quadratic coefficient. Our error estimate of adjusted GMSL is derived incorporating the variability inherent to the time series itself with uncertainty in mission-specific bias drift and relative bias estimates using a Monte Carlo approach with 1,000 iterations. This approach yields a standard deviation of GMSL trends of ±0.37 mm/yr. We add in quadrature to this term uncertainties associated with the reference frame, specifically those associated with the Z-rate and scale-rate of the ITRF. The estimated uncertainty of the Z-rate is 0.45 mm/yr[42], however, given the asymmetric distribution of the oceans, only ~12% of this error will manifest in GMSL[37], i.e. ±0.05 mm/yr. Uncertainties in X- and Y-rates of geocentre are much smaller and have negligible contribution. Uncertainty associated with the scale-rate is between ±0.18-0.3 mm/yr[42-44]. We adopt ±0.25 mm/yr for this term and make the conservative assumption it will propagate at 100% into GMSL. The final uncertainty for our adjusted linear rate of GMSL change is therefore ±0.449 mm/yr which is rounded to ±0.4 mm/yr (in close agreement with refs

6 and 7). For comparison, if we follow the same process but exclude the bias drift uncertainties in the Monte Carlo estimation (i.e. only consider relative bias and frame uncertainties, in addition to variability in the time series itself), the final GMSL rate uncertainty is reduced to ±0.329 mm/yr (rounding to ±0.3 mm/yr). Regarding the uncertainty for the quadratic term, the same Monte Carlo approach is taken, however the reference frame terms are excluded given they are assumed to only affect the rate. The uncertainty of the quadratic term is ±0.029 mm/yr^2 (later doubled to reflect uncertainty in acceleration).

Supplementary Discussion

Characterisation and Attribution of the TOPEX Side A Bias Drift

Our a priori assumption, when estimating bias drift, is the use of a linear model for each satellite mission (see Supplementary Methods, Eqn 5) as also adopted in earlier studies[5,15]. Residuals about this linear model from each CP are stacked on a cycle-by-cycle basis using the same weighting strategy as per the mission-wise bias drift estimates (Eqn 6), allowing the formation of a residual bias time series (Supplementary Figure 3). By definition, these residual time series have zero trend when estimated taking into account the cycle-by-cycle uncertainty.

The residual time series for TOPEX side A (Supplementary Figure 3) shows the greatest variability (RMS 6.12 mm vs 5.11 mm (TOPEX side B), 4.77 mm (Jason-1) and 4.92 mm (OSTM/Jason-2) respectively). Non-linearity within the residuals for TOPEX side A suggests the linear model is inadequately describing the true behavior of time-variable biases within the measurement system. In the absence of a physical basis to describe a more complex functional model, we chose to test a piecewise linear approach for TOPEX side A. We modified the parameterization provided in Eqn 5 to include three linear coefficients (P1, P2 and P3) describing successive piecewise linear trends following a single (existing) constant intercept (offset) parameter. The transition times for the piecewise linear terms were determined simply by dividing the side A record into three equal length sub-sets (each approximately 2.05 yr duration). Results for this parameterization (Supplementary Table 1) are unsurprisingly more uncertain, yet reveal significant changes in the bias drift over the three time periods. The residual RMS using the piecewise approach (5.37 mm) is now closer to that of side B using a linear model (5.11 mm), yet there remains clear structure within the residuals (Supplementary Figure 3). Application of the piecewise linear results to derive an adjusted GMSL curve (in conjunction with the linear bias

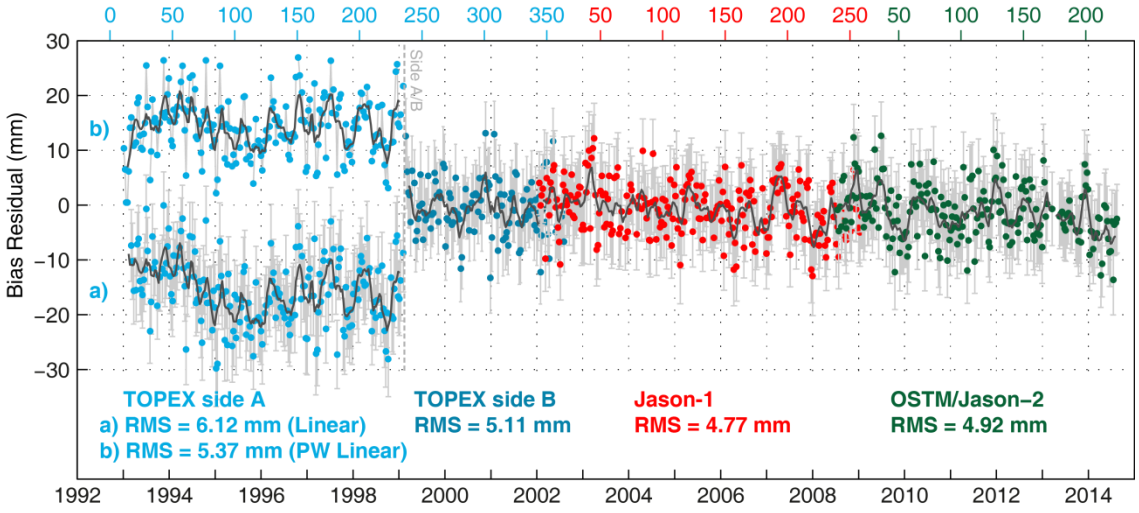

Supplementary Figure 3. Cycle-by-cycle residuals from the bias drift estimation for each mission. Two variants are shown for TOPEX side A based on a linear model for bias drift (a) and an extended piecewise (PW) linear model (b), each offset by ± 15 mm for clarity, respectively (see Supplementary Discussion for details of the extended model). Note by definition the weighted regression of the residual time series yields zero slope.

drift estimates for TOPEX side B, Jason-1 and OSTM/Jason-2) slightly reduces the overall multi-mission rate of GMSL rise to +2.4 ± 0.5 mm/yr (note the increase in uncertainty as derived from an updated Monte Carlo analysis). The acceleration term is marginally increased to +0.057 ± 0.088 mm/yr^2 (note the uncertainty has been doubled to reflect the uncertainty in acceleration, not the quadratic coefficient).

Supplementary Table 1. Comparison of results using different parameterisation for the TOPEX side A bias drift (recall all uncertainties are 1-sigma estimates).

Parameter	Piecewise Linear Model	Linear Model
Bias Drift	P1: -2.82 ± 1.56 mm/yr P2: +2.68 ± 1.32 mm/yr P3: +1.12 ± 1.61 mm/yr	+1.49 ± 0.49 mm/yr
TOPEX side A Residual RMS	5.37 mm	6.12 mm
TOPEX side B-A Relative Bias	+0.8 ± 5.1 mm	-2.9 ± 2.5 mm
Adjusted GMSL Rate	+2.4 ± 0.5 mm/yr	+2.6 ± 0.4 mm/yr
Adjusted GMSL Acceleration	+0.057 ± 0.088 mm/yr^2	+0.041 ± 0.058 mm/yr^2

The TOPEX side A residual bias time series (Supplementary Figure 3) suggests the time variable nature of the bias drift is complex. The piecewise linear model reduced variability within the residual time series, yet only marginally changed the adjusted GMSL rate and acceleration

from that determined using the linear model (Supplementary Table 1). In the absence of further information to characterize the bias drift (which may well include small offsets and nonlinear terms), we maintain the use of the linear model across all missions.

To further test sensitivity to TOPEX side A, removing 1.5 years of data from the end of the record, when side A experienced performance degradation, has the effect of reducing the side A bias drift by ~38% to +0.93 ± 0.68 mm/yr. Alternatively, excluding all 1993 data (as undertaken in ref 1 when computing GMSL trends) increases the side A bias drift to +1.95 ± 0.66 mm/yr (consistent with the findings from the piecewise linear analysis, Supplementary Table 1). We also compute bias drift estimates for a number of variant TOPEX datasets, retaining the same method and estimation strategy, thus providing an ability to test sensitivity. When we use modelled wet and dry troposphere corrections obtained from the ERA or NCEP models available from the Radar Altimeter Database System, TOPEX side A bias drift reduces to +1.00 ± 0.51 mm/yr and +0.98 ± 0.54 mm/yr respectively (compared to +1.49 ± 0.49 mm/yr for our preferred solution). Note the marginal increase in bias drift uncertainty when using the modelled products. Using the ERA product and +1.00 mm/yr as the TOPEX side A bias drift has the effect of marginally lifting the adjusted GMSL rate from +2.55 to +2.64 mm/yr. Unadjusted and adjusted GMSL trends computed over just the TOPEX period highlight the influence of the different treatments for the tropospheric delay (Supplementary Figure 4). Note the adjusted trends show much lower variability (Supplementary Figure 4). These results suggest there is some residual bias in the calibration and characterization of satellite yaw dependent effects on the satellite, including its effect on the TMR instrument (see ref 45 for further discussion regarding the use of modelled products for the correction of the tropospheric wet path delay).

Counter intuitively, when we process TOPEX side A data derived from standard MGDR-B data (i.e. using orbit, wet, dry and SSB data as per the MGDR-B release without further correction), the resultant bias drift is +0.17 ± 0.49 mm/yr. This result is however partly misleading given differences in the reference frame used in the orbits, and other inhomogeneities across the "standard" MGDR-B dataset. Note that the adjusted GMSL trend when using data and bias drift estimates derived from standard release GDR data is +2.7 ± 0.4 mm/yr, only marginally higher than our preferred rate of +2.6 ± 0.4 mm/yr (see also Supplementary Figure 4).

Despite observing a clear dependence of the TOPEX intra-mission relative bias on the choice of SSB model (see following section), we observe only negligible difference in the bias drift estimates (+1.37 ± 0.49 mm/yr when using the Tran et al. SSB[34], vs +1.49 ± 0.49 mm/yr when using the preferred Chambers et al. SSB[33]).

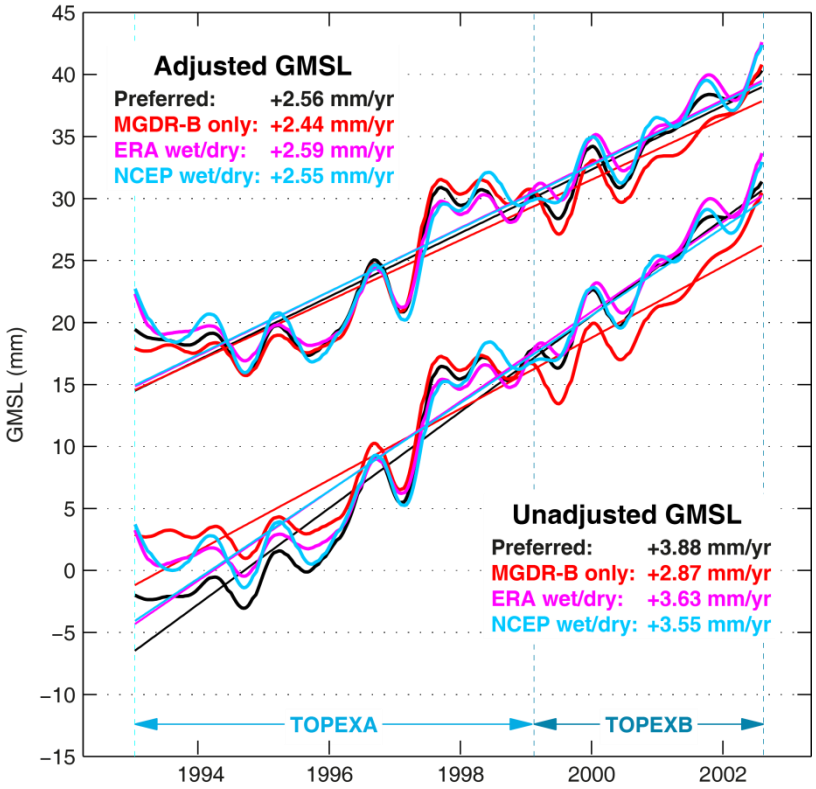

Supplementary Figure 4. Unadjusted (bottom grouping) and adjusted (top grouping) GMSL time series (60 day filtered, annual and semi-annual removed) spanning the TOPEX period only showing the influence of different altimeter data processing selections. The rates shown span just the TOPEX side A and B period. The "preferred" dataset (black) is as per Figure 3. "MGDR-B only" (red) is the conventional MGDR-B data without further correction. "ERA wet/dry" (magenta) uses ERA wet and dry tropospheric corrections (orbits and SSB as per preferred time series). "NCEP wet/dry" (cyan) uses NCEP wet and dry tropospheric corrections (orbits and SSB as per preferred time series).

Finally, we applied our approach to the most recent release of along-track TOPEX, Jason-1 and OSTM/Jason-2 data provided by the University of Colorado (CU) for comparative purposes (see ref 3 for examples of differences between our (CSIRO) and CU GMSL time series). Results for the TOPEX side A and B bias drifts were comparable (+1.02 ± 0.51 mm/yr and +1.05 ± 0.96 mm/yr respectively), suggesting small differences in bias drift as a function of subtle differences in side A processing. These results do however suggest that the majority of the TOPEX drift is independent of the along-track processing method used to generate either the CU or our altimeter SSH data. We note that the unadjusted and adjusted GMSL trends for the CU data were within 0.02 and 0.06 mm/yr of our values, respectively (Figure 3).

TOPEX Side A/B Intra-mission Relative Bias

The TOPEX side B minus TOPEX side A intra-mission relative bias is vital in generating a multi-mission GMSL time series yet remains problematic given the lack of overlapping formation flight data as per the other missions (see later). We are able to compute the A/B relative bias and compare results with those found in the literature. We observe this relative bias to be dependent on the choice of the sea state bias (SSB) model used in deriving SSH. Our preference is the application of the Chambers et al. SSB[33], yielding a relative bias of -2.9 ± 2.5 mm (in close support of the result by ref 33), noticeably lower than -7.6 ± 2.5 mm when using the Tran et al. SSB[34]. The Tran et al. SSB remains the model of choice for Jason-1 and OSTM/Jason-2.

As discussed previously, when using the more sophisticated piecewise linear model for TOPEX side A bias drift, the A/B relative bias (using the Chambers et al. SSB[33]) is +0.8 ± 5.1 mm, consistent with the more precise estimate from the linear model of -2.9 ± 2.5 mm. We note that changing the A/B relative bias by 1 mm introduces a change in the GMSL rate of 0.059 mm/yr over the duration of the record, underscoring its importance in deriving a GMSL time series. Forcing the relative bias to 0.0 mm, rather than the estimated value of -2.9 mm, decreases the estimated rate of GMSL by 0.16 mm/yr (i.e. 2.39 mm/yr compared with 2.55 mm/yr for the adjusted case using GPS-based VLM).

Inter-mission Relative Biases

Our estimates of inter-mission relative biases derived from the average of CP based estimates weighted using the same strategy as for the bias drift estimation process, agree to within estimated errors when compared to estimates derived from cycle-by-cycle comparison of overlapping (so called "formation flight") altimeter data (Supplementary Table 2). Inter-mission relative bias estimates from our computational approach are used when forming our adjusted GMSL time series.

Supplementary Table 2. Relative biases (mm) determined from current strategy vs global means of cycle-by-cycle differences over formation flight periods.

Jason-1 – TOPEX side B		**OSTM/Jason-2 – Jason-1**	
Our Approach	Global Mean	Our Approach	Global Mean
+86.1 ± 2.0 mm	+85.9 ± 1.2 mm	-73.8 ± 1.5 mm	-73.2 ± 0.5 mm

Bias Drift Sensitivity

After cumulatively removing up to the top 20% of highest weighted (lowest uncertainty) CPs from the estimation process, bias drift results remain unchanged to within about 0.2 mm/yr (Supplementary Figure 5). These top 20% of CPs include contributions from ~48% of the TGs in the solution. Removal of the bottom quartile of CPs changes the results across all missions by between -0.06 and +0.17 mm/yr. The relative insensitivity of our approach to poorly behaving sites is illustrated when the 26 TGs identified as being susceptible to earthquakes were included; results were affected by no more than 0.28 mm/yr, a major improvement compared to the standard approach[17].

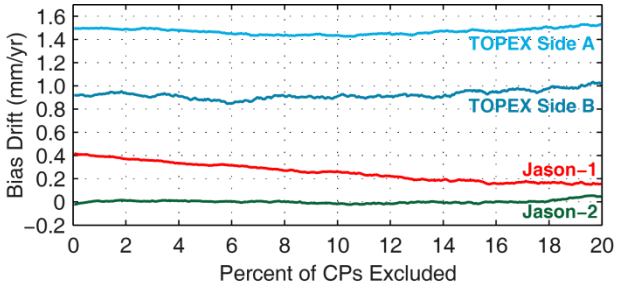

Supplementary Figure 5. Bias drift estimates (coloured lines) as a function of the percentage of the dataset excluded from the estimation process, with data sorted from most to least precise (highest to lowest weight). 20% of the dataset corresponds to bias drift estimates from ~450 CPs.

In order to further assess sensitivity of our results, we determine bias drift for each mission using the same weighting strategy but limiting input data to CPs associated with 1) TGs located on islands and 2) TGs located or on/adjacent to continents (Supplementary Table 3). Approximately 42% of data is derived from TGs located on islands. We observe no systematic effect for TOPEX side A, Jason-1 and OSTM/Jason-2 when comparing drift estimates computed from island only TGs vs continental only TGs. TOPEX side B seems most sensitive to this variation in the TG network; however, we note this is the shortest mission with corresponding largest uncertainty for bias drift estimates. In all cases, this variation in the TG network increases uncertainty given the large reduction in sample size.

Supplementary Table 3. Mission-wise bias drift estimates (GPS-based VLM) for island only, continental only, and all TG locations, with adjusted GMSL trend estimates shown in right hand column. Numbers in brackets refer to number of TGs in solution.

TG Location	Bias Drift (mm/yr)				Adjusted GMSL (mm/yr)
	TOPEX side A	TOPEX side B	Jason-1	OSTM/Jason-2	
Island Only	1.69 ± 0.69 (39)	-0.01 ± 1.20 (40)	0.84 ± 0.65 (41)	+0.00 ± 0.69 (40)	+2.5 ± 0.6
Continental Only	1.07 ± 0.73 (51)	2.90 ± 1.49 (55)	-0.35 ± 0.49 (60)	-0.06 ± 0.58 (50)	+2.5 ± 0.6
All	**1.49 ± 0.49 (90)**	**0.93 ± 0.92 (95)**	**0.42 ± 0.41 (101)**	**-0.02 ± 0.44 (90)**	**+2.6 ± 0.4**

Given our approach to handling the residual ocean tide between the TG and CP is different to that used in the established methodology (e.g. refs 6,7,22), we investigated the sensitivity of alternate approaches (e.g. using a global tide model at the CP, and a full harmonic analysis at the TG, or a tide model at the CP, but monthly moving average at the TG). In each case, the variability in the bias residual (e.g. Supplementary Figure 3) increases by up to ~40% from our preferred approach, in which the residual tide is estimated from the ensemble altimeter minus TG time series (Eqn 5). Bias drift estimates computed with the alternate approaches differ on average by ~0.1 mm/yr, up to 0.25 mm/yr, compared with those computed using the preferred technique. Given the increased variability associated with the alternative approaches, there is a commensurate increase in the bias drift uncertainty.

Finally, we tested sensitivity to two slightly different treatments of VLM. First, we computed bias drift estimates using only those TGs with GPS VLM available within 100 km (i.e. all TGs without GPS-based VLM were excluded). This solution reduces the sample size to 69% of the original TG network, leading to increased uncertainties for all missions (Supplementary Table 4). The effect of this variant is to further increase each bias drift estimate, subsequently reducing the adjusted GMSL trend by 0.22 mm/yr (Supplementary Table 4). We contend that the most robust solution will have as many TGs as possible to minimize any influence of network geometry. For this reason, we prefer reverting to GIA plus elastic VLM where GPS is unavailable.

Supplementary Table 4. Comparison of results using GPS VLM (or GIA plus elastic VLM where GPS is unavailable) and GPS-only VLM.

Mission	GPS (or GIA plus elastic) VLM	GPS-only VLM
TOPEX-A	+1.49±0.49 mm/yr	+1.87±0.55 mm/yr
TOPEX-B	+0.93±0.92 mm/yr	+1.08±1.09 mm/yr
Jason-1	+0.42±0.41 mm/yr	+0.72±0.46 mm/yr
Jason-2	-0.02±0.44 mm/yr	+0.43±0.50 mm/yr
Adjusted GMSL:	2.56±0.37 mm/yr	2.34±0.41 mm/yr

Second, we tested an alternate GIA model (ref 46) to assess possible variation in bias drift estimates when applying solely GIA-based VLM. Results using this model compared to those computed using the ICE-5G VM2 L90 model were within 0.05 mm/yr for all missions.

Multi-mission Ensemble Bias Drift Determination

As a final check on the robustness of our technique, we compute a single bias drift estimate per CP using the ensemble (i.e. full two decade record) multi-mission SSH time series derived from the TOPEX side A, TOPEX side B, Jason-1 and OSTM/Jason-2 records. This process requires the addition of intra- and inter-mission relative bias parameters in Eqn 5, but otherwise the estimation process closely follows the previous approach. Results (Supplementary Table 5) show that the multi-mission record overestimates the trend in GMSL depending on the choice of VLM applied. These results are closely consistent with the adjusted GMSL curves that take into account the individual mission bias drifts (Figures 2 and 3).

Supplementary Table 5. Multi-mission (TOPEX side A and B, Jason-1 and OSTM/Jason-2) bias drift (mm/yr) as a function of VLM applied in the estimation strategy. Note that in the case of GPS VLM, if GPS estimates are unavailable for a specific TG, GIA+Elastic VLM is substituted.

VLM Applied	Multi-mission Bias Drift (mm/yr)
None	+0.05 ± 0.24
GIA+Elastic	+0.38 ± 0.23
GPS (see caption)	+0.70 ± 0.22

A mis-closure test was also applied using the multi-mission data. For this test, we commence by generating an adjusted multi-mission record by applying our preferred bias drift estimates (for a given VLM treatment) for each mission. Using this adjusted multi-mission time series, we then estimate bias drift over the complete period with respect to TGs using the same VLM treatment in the estimation process. Given the input time series is adjusted using mission-specific bias drift estimates derived using the same VLM, the bias drift of the multi-mission record should equal zero. Results support this hypothesis (Supplementary Table 6).

Supplementary Table 6. Mis-closure tests: Bias drift estimates (mm/yr) using adjusted multi-mission data with the same VLM strategy adopted for the adjustment and subsequent bias drift estimation process (hence bias drift estimates should be equal to zero). Note that in the case of GPS VLM, if GPS estimates are unavailable for a specific TG, GIA+Elastic VLM is substituted.

VLM Applied (Adjustment)	VLM Applied (Estimation)	Multi-mission Bias Drift (mm/yr)
GIA+Elastic	GIA+Elastic	+0.11 ± 0.25
GPS (see caption)	GPS (see caption)	+0.15 ± 0.23

GMSL Comparisons

Our unadjusted estimate of the rate of change of GMSL from the Jason-class missions (1993 to mid-2014) is +3.2 ± 0.3 mm/yr and identical or very close to other published rates[1-3]. Following the adjustment for bias drift, this changes to +3.0 ± 0.4 mm/yr (GIA VLM), +2.9 ± 0.4 mm/yr (GIA plus elastic VLM), to +2.6 ± 0.4 mm/yr (GPS-based VLM), noting that all estimates have been corrected for the change in volume of the ocean basins caused by GIA (+0.33 mm/yr), as well as for the inverse barometer effect. The adjusted rate of GMSL using bias drift estimates computed without any VLM is +2.8 ± 0.4 mm/yr. Given this estimate has no VLM applied at the TGs, the GMSL rate has not been adjusted for the GIA induced change to the ocean basins. Calibrating for bias drift without application of VLM at TGs should yield an altimeter derived rate of change in GMSL that is effectively representative of changing ocean volume, providing the TG network is sufficiently well distributed as to adequately sample the oceanic GIA signal (the error in this assumption for TG-based estimates of GMSL is discussed by ref 47; however, is not important here as this result is only computed for illustrative purposes).

Our adjusted GMSL rates are in closer agreement with the trend in GMSL computed from a comprehensive network of TGs alone (+2.7 ± 0.6 mm/yr, updated from ref 8, 1993 to end 2012,

with the same GPS-based VLM taken into consideration to yield a change in ocean volume. Note there is significant difference in the tide gauge network used to estimate GMSL (up to 400 TGs[8]) compared with that used to compute bias drift estimates (96 TGs)). It is also consistent with updated estimates of the sum of observed contributions to GMSL over 1993 to end 2009, which sum to +2.8 ± 0.5 mm/yr (ref 2). Rates of change in GMSL computed from other satellite missions (e.g. EnviSat/ERS1&2) are typically highly uncertain given an ongoing effort in the community to homogeneously reprocess often problematic data from these missions. The ERS-2 mission (1995 to end 2003) spans much of the TOPEX record and therefore may be informative given the suggested bias drift we observe in the TOPEX data. Ref 9 provides a linear rate of GMSL change computed from recently reprocessed ERS-2 data of +2.5-2.7 mm/yr, which agrees favourably with our adjusted rate computed over the same time period of +2.8 mm/yr. Note over the same period, our unadjusted rate of +3.99 mm/yr is significantly higher. Note that the uncertainty of ± 0.2 mm/yr quoted for the ERS-2 trend estimates[9] simply reflect formal errors from a least squares fit and are likely optimistic.

Supplementary References

31 Brown, S. A novel near-land radiometer wet path-delay retrieval algorithm: Application to the Jason-2/OSTM Advanced Microwave Radiometer. *IEEE Transactions on Geoscience and Remote Sensing* **48**, 1986-1992, doi:10.1109/TGRS.2009.2037220 (2010).

32 Leuliette, E. W., Nerem, R. S. & Mitchum, G. T. Calibration of TOPEX/Poseidon and Jason altimeter data to construct a continuous record of mean sea level change. *Marine Geodesy* **27**, 79-94, doi:10.1080/01490410490465193 (2004).

33 Chambers, D. P., Hayes, S. A., Ries, J. C. & Urban, T. J. New TOPEX sea state bias models and their effect on global mean sea level. *Journal of Geophysical Research* **108**, doi:10.1029/2003JC001839 (2003).

34 Tran, N. *et al.* Sea state bias in altimeter sea level estimates determined by combining wave model and satellite data. *Journal of Geophysical Research* **115**, doi:10.1029/2009JC005534 (2010).

35 Lemoine, F. G. *et al.* Towards development of a consistent orbit series for TOPEX, Jason-1, and Jason-2. *Advances in Space Research* **46**, 1513-1540, doi:10.1016/j.asr.2010.05.007 (2010).

36 Williams, S. D. P. CATS: GPS coordinate time series analysis software. *GPS Solutions* **12**, 147-153, doi:10.1007/s10291-007-0086-4 (2008).

37 Morel, L. & Willis, P. Terrestrial reference frame effects on global sea level rise determination from TOPEX/Poseidon altimetric data. *Advances in Space Research* **36**, 358-368, doi:10.1016/j.asr.2005.05.113 (2005).

38 Holland, P. W. & Welsch, R. E. Robust regression using iteratively reweighted least-squares. *Communications in Statistics - Theory and Methods* **6**, 813-827, doi:10.1080/03610927708827533 (1977).

39 Dziewonski, A. M., Chou, T. A. & Woodhouse, J. H. Determination of earthquake source parameters from waveform data for studies of global and regional seismicity. *Journal of Geophysical Research* **86**, 2825-2852, doi:10.1029/JB086iB04p02825 (1981).

40 Pollitz, F. F. Coseismic Deformation From Earthquake Faulting On A Layered Spherical Earth. *Geophysical Journal International* **125**, 1-14, doi:10.1111/j.1365-246X.1996.tb06530.x (1996).

41 Tregoning, P. *et al.* A decade of horizontal deformation from great earthquakes. *Journal of Geophysical Research: Solid Earth* **118**, 2371-2381, doi:10.1002/jgrb.50154 (2013).

42 Argus, D. F. Uncertainty in the velocity between the mass center and surface of Earth. *Journal of Geophysical Research B: Solid Earth* **117**, doi:10.1029/2012jb009196 (2012).

43 Collilieux, X. *et al.* in *Earth on the Edge: Science for a Sustainable Planet* Vol. 139 *International Association of Geodesy Symposia* (eds Chris Rizos & Pascal Willis) Ch. 25, 197-202 (Springer Berlin Heidelberg, 2014).

44 Wu, X. *et al.* Accuracy of the International Terrestrial Reference Frame origin and Earth expansion. *Geophysical Research Letters* **38**, L13304, doi:10.1029/2011GL047450 (2011).

45 Legeais, J. F., Ablain, M. & Thao, S. Evaluation of wet troposphere path delays from atmospheric reanalyses and radiometers and their impact on the altimeter sea level. *Ocean Sci.* **10**, 893-905, 10.5194/os-10-893-2014 (2014).

46 Paulson, A., Zhong, S. & Wahr, J. Inference of mantle viscosity from GRACE and relative sea level data. *Geophysical Journal International* **171**, 497-508, 10.1111/j.1365-246X.2007.03556.x (2007).

47 Jevrejeva, S., Moore, J. C., Grinsted, A., Matthews, A. P. & Spada, G. Trends and acceleration in global and regional sea levels since 1807. *Global and Planetary Change* **113**, 11-22 (2014).